JGR Atmospheres

RESEARCH ARTICLE
10.1029/2021JD034972

The Response of Daily and Sub-Daily Extreme Precipitations to Changes in Surface and Dew-Point Temperatures

Alexis Pérez Bello[1], **Alain Mailhot**[1], **and Dominique Paquin**[2]

[1]Center Eau Terre Environnement (INRS-ETE) Québec, Institut National de la Recherche Scientifique, Québec City, QC, Canada, [2]Consortium on Regional Climatology and Adaptation to Climate Change (Ouranos), Montréal, QC, Canada

Key Points:

- Temperature-precipitation scaling using surface dew-point temperature provides more robust estimates compared to surface air temperature
- The link between extreme precipitation and surface dew-point temperature (SDPT) changes is more robustly constrained for short-duration events and the future period
- The scaling using SDPT in historical period can be used to estimate changes in rainfall extremes in the future over most of the domain

Supporting Information:

Supporting Information may be found in the online version of this article.

Correspondence to:

A. Pérez Bello,
alexis.perez_bello@ete.inrs.ca

Citation:

Pérez Bello, A., Mailhot, A., & Paquin, D. (2021). The response of daily and sub-daily extreme precipitations to changes in surface and dew-point temperatures. *Journal of Geophysical Research: Atmospheres*, *126*, e2021JD034972. https://doi.org/10.1029/2021JD034972

Received 25 MAR 2021
Accepted 2 AUG 2021

Abstract Extreme precipitation events are expected to increase in frequency and intensity in the future climate, but the magnitude of these changes remains uncertain. The relationship between extreme precipitation and the surface temperature has been investigated to more robustly assess projected increases in extreme precipitation considering that projected temperature is more adequately simulated. Relationships between extreme precipitation (daily and sub-daily) and surface air temperature (SAT) or surface dew-point temperature (SDPT) are analyzed in this study using the 50-members ensemble from the fifth version of the Canadian Regional Climate Model covering the Northeastern North America region over the period 1956–2099. Temperature-precipitation scaling rates (TPSRs) were estimated using local SAT and SDPT seasonal anomalies as covariate over both periods for 2–100-year extreme precipitation events and durations ranging from 1 to 24 h. Contrasting responses were obtained when using SAT or SDPT, especially in the southern part of the domain. Median scaling rates over the entire domain for SDPT were close to the Clausius-Clapeyron scaling (≈7% /°C) while they were much smaller for SAT and even negative in southern regions, showing that moisture availability is a key factor for these regions. TPSR based on SDPT is also more robustly constrained and can be used to estimate changes in short-duration extreme precipitation in a future period from TPSR in the historical period over a large part of the domain.

Plain Language Summary Extreme precipitation events are expected to be more intense and frequent in the future. The magnitude of these changes remains, however, uncertain. It is also possible to relate extreme precipitation changes to changes in surface temperature. The basic idea is that a warmer atmosphere can hold more moisture and therefore trigger more intense precipitation. Such a relationship can estimate future changes in extreme precipitation since simulated temperature from climate models is more reliable than precipitation. The response of extreme precipitation events to changes in surface air temperature and the surface dew-point temperature was analyzed over the Northeastern North America region using a large ensemble of 50 climate simulations covering the period 1956–2099. It was shown that more robust estimates of the temperature-precipitation relationship are obtained when using the surface dew-point temperature, confirming that available moisture can be a limiting factor in increasing extreme precipitation for some regions. Those estimates were consistent between the historical and future climate over a large part of the study region for the more extreme events and confirm that future extreme precipitation changes can be estimated from changes in dew-point temperature.

1. Introduction

Extreme precipitation events are expected to increase in frequency and intensity in a future climate under warmer conditions (IPCC, 2014). Many observational and modeling-based studies support this conclusion (Alexander et al., 2006; Donat et al., 2013; Fischer & Knutti, 2016; Frich et al., 2002; Gutowski et al., 2007; Kharin et al., 2013; Li et al., 2021; Mailhot et al., 2011; Min et al., 2011; Sun et al., 2021). Despite the increasing scientific evidence, there are still many uncertainties on the magnitude and the physical processes conditioning these changes (Lenderink & Meijgaard, 2008; Westra et al., 2014).

The relationship between extreme precipitation and surface temperature has been studied to assess how extreme precipitation may change under warming conditions. Given that projections on temperature are

considered to be more reliable than those for extreme precipitation (Räisänen, 2007), temperature-precipitation (T-P) relationships were analyzed to obtain more robust extreme precipitation projections (X. Zhang et al., 2017; W. Zhang et al., 2019). However, linking temperature fields with extreme rainfall is not straightforward since many factors (e.g., regional weather patterns, extreme precipitation percentile, seasons, timescale, and rainfall type) may also influence this relationship (Martinkova & Kysely, 2020; Panthou et al., 2014; Westra et al., 2014). Many studies have investigated T-P relationship in observed (e.g., Hardwick Jones et al., 2010; Lenderink & Meijgaard, 2008, 2010; Lenderink et al., 2017; Panthou et al., 2014; Utsumi et al., 2011), and simulated data (e.g., Lenderink et al., 2021; O'Gorman, 2012; O'Gorman & Schneider, 2009) to better understand the involved processes and improve our confidence in extreme precipitation projections (for a review of such studies in mid-latitude regions see Martinkova & Kysely, 2020).

T-P relationship is often explained through the dependence between increasing air temperature and the atmosphere's higher water-holding capacity as described by the Clausius-Clapeyron (CC) equation. Under certain assumptions (e.g., unchanged relative humidity and no significant changes in atmospheric circulation; Lenderink & Meijgaard, 2008), it is expected that the changes in extreme precipitation intensities should follow the rate of change of the atmosphere water-holding capacity with temperature as defined by the CC relationship (≈7% /°C, hereafter called the CC scaling; Trenberth et al., 2003). These thermodynamically induced changes are expected to dominate for more extreme precipitation events in the mid-to-high latitudes (Emori & Brown, 2005; Norris et al., 2019; Pfahl et al., 2017). In contrast, circulation changes may weaken extreme precipitation or, on the opposite, enhanced such events by increasing moisture supplies and resulting in a super CC scaling rate (defined here as temperature scaling above the CC scaling).

Different statistical approaches have been used to investigated T-P relationship, the most common one being the binning approach or binning technique (Ali et al., 2018; Lenderink & Meijgaard, 2008; Martinkova & Kysely, 2020). According to this approach, rainfall records are partitioned into temperature bins and the precipitation intensities corresponding to specific percentiles within each bin are estimated (e.g., 95^{th}, 99^{th} or 99.9^{th}). These bins can be defined using fixed-width (Lenderink & Meijgaard, 2008), with an overlap (Lenderink et al., 2011) or using a given number of bins with the same number of samples within each bin (Bao et al., 2017; Hardwick Jones et al., 2010). Quantile regression was also proposed (Wasko & Sharma, 2014), which is not affected by assumptions about the sample size. No significant difference between quantile regression and binning approach was observed for large samples (Wasko & Sharma, 2014).

The binning approach has been, however, subject to some criticism. Bao et al. (2017) found that this method was not appropriate to link warming to changes in extreme precipitation. These authors found that during precipitation events in Darwin (Australia), fast cooling of surface air temperature (SAT) was observed, therefore influencing the scaling (negative scaling rate) by shifting many events to cooler temperature bins. X. Zhang et al. (2017) also argued that seasonal variations affect extreme precipitations as well as temperature. Therefore, the expected evolution of extreme rainfall events in a warming climate cannot be projected from the binning scaling because seasonality influences both variables (temperature and rainfall) and excludes a causal relationship between them. Furthermore, X. Zhang et al. (2017) argued that most of these extremes are not annual rainfall extremes because the precipitation values are conditional on observed temperature, calling these "conditional quantiles." The binning approach was also applied to a convection-permitting simulation by Prein et al. (2017) over the United States. A shift of the binning curves along the CC scaling in future climate was observed. Sun et al. (2020) using a large ensemble from the Canadian regional climate model (CanRCM4) also found that the binning scaling did not provide reliable projections of extreme precipitation.

X. Zhang et al. (2017) proposed an approach where hourly maximum precipitation events for each summer (June-July-August) are extracted over a specific period, and then normalized by the summer median values. These normalized data were then adjusted to the generalized extreme value (GEV) distribution using seasonal temperature anomalies (e.g., summer temperature) as a covariate for the GEV location parameter or both, the GEV location and scale parameters. Finally, the temperature-precipitation scaling rate (TPSR) was estimated as the changes in the 50th percentile return level (2-year event). Such procedure is intended to condition extreme precipitation on seasonal temperature rather than daily mean temperature. Ali et al. (2018) compared the X. Zhang et al. (2017)'s method to binning and quantile regression methods using worldwide observational records. These authors fitted a GEV distribution to the normalized daily maximum

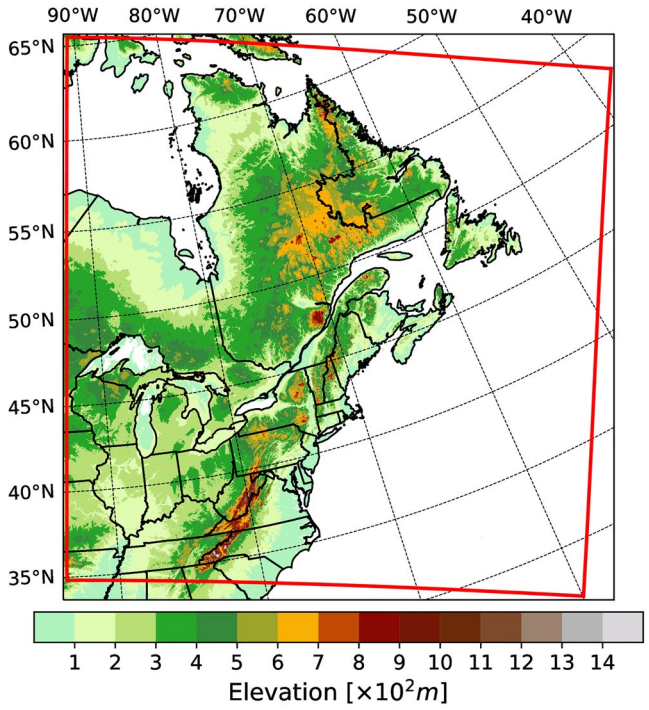

Figure 1. Map of the study region (Northeastern North America [NNA]). Colors represent the altitude (in meters), and the red lines delineate the Canadian Regional Climate Model-Large Ensemble simulation domain.

precipitation events over the four months with the highest precipitation (site-dependant), using surface air and dew-point temperatures anomalies as covariates for the GEV location parameter. They concluded that more robust estimates of the scaling rates were obtained when using the X. Zhang et al. (2017)'s method.

Another key factor in the extreme precipitation generation process is the atmospheric moisture availability (Trenberth et al., 2003). Berg et al. (2009) found that it was the limiting factor for summer rainfall intensity at a daily time scale in Europe. Furthermore, Hardwick Jones et al. (2010) observed a decrease in the relative humidity at higher temperatures over Australia. Lenderink and Meijgaard (2010) therefore proposed to use dew-point temperatures instead of surface temperature to account for the available moisture in the atmosphere, thus eliminating the assumption that relative humidity remained unchanged with temperature (Lenderink & Attema, 2015). These authors showed that dew-point temperature is a better indicator of changes in extreme precipitation events (Lenderink et al., 2017; Roderick et al., 2020). In Canada, Panthou et al. (2014) found that the relative humidity was a limiting factor for inland regions while it was not for coastal regions. Limited moisture availability at higher temperatures was also observed by Molnar et al. (2015) in Switzerland, Park and Min (2017) in South Korea, and Peleg et al. (2018) in the eastern Mediterranean. Finally, it should be mentioned that, contrary to previous studies, Visser et al. (2020) argued that dry-bulb temperature can adequately describe short-duration extreme precipitation if sub-daily atmospheric conditions before the storm events are taken into consideration.

In this paper, we study how sub-daily extreme precipitation will change under global warming by using a unique large ensemble of regional climate simulations. Robustly constrained scaling relationships between precipitation extremes and SAT or surface dew-point temperature (SDPT) are investigated and compared over historical and future climate. The scaling relationships in historical climate to assess future changes in extreme precipitation are also evaluated. Hence, the objective of this study is two-fold. First, it investigates how daily and sub-daily extreme precipitation responds to changes in SAT and SDPT over the Northeastern North America region in current and future climates using a 50-members regional climate model large ensemble. The robustness of the scaling rates estimated using SDPT and SAT is compared. Second, the possibility to use scaling rates in the historical period to estimate future changes in precipitation extremes is analyzed.

2. Data Sets and Methods

2.1. Regional Climate Model Ensemble

A 50-members ensemble simulation from the fifth version of the Canadian Regional Climate Model-Large Ensemble (CRCM5-LE) (Martynov et al., 2013; Separović et al., 2013) over the period 1956–2099 was used (Leduc et al., 2019). The CRCM5-LE has a spatial resolution of 0.11° (around 12 km) and covers the Northeastern North America (NNA) region (Figure 1). This data set is a dynamically downscaled version of the 50-member Canadian Earth System Model version 2-Large Ensemble (CanESM2-LE) (Arora et al., 2011; Fyfe et al., 2017) with ∼310 km of spatial resolution using observed greenhouse gases emissions up to the year 2005 and forcing scenario RCP8.5 (Representative Concentration Pathways) from 2006 to 2099 (Leduc et al., 2019). The simulations started in 1950, but the first 6-year period was discarded as a spin-up period. Each simulation (member) is assumed to be an independent realization of the climate system (Leduc et al., 2019). An advantage of this large ensemble is the possibility to study rare and more extreme events. It should also be mentioned that convective processes are parameterized in CRCM5-LE.

The performance of this data set in simulating the spatio-temporal structure of extreme precipitation over the NNA domain was investigated by Innocenti, Mailhot, Frigon, et al. (2019) as well as the response of daily and sub-daily precipitation extremes to future warming conditions (Innocenti, Mailhot, Leduc, et al., 2019). Martel et al. (2020) also evaluated the future changes in the frequency and intensities of extreme precipitations using this ensemble. Overall, this data set provides an improved representation of local extreme precipitation events and temperature variability when compared to global climate models (Leduc et al., 2019).

2.2. Temperature-Precipitation Scaling Rate Estimation

Three variables from the CRCM5-LE simulations were used: (a) 1-h total precipitation, (b) 3-h SAT, and (c) 3-h Surface Relative Humidity. The 3-h SDPT series were estimated using the equation proposed by Alduchov and Eskridge (1996) and Lawrence (2005) (see Equation S1).

TPSRs were estimated using the approach proposed by X. Zhang et al. (2017). The five months (May-June-July-August-September) with the highest probability of occurrence of hourly annual maximum precipitation over the study domain were considered. May to September 6, 12, and 24 h annual maxima precipitation series were therefore extracted from simulated hourly precipitation. Seasonal (May–September) mean temperatures (SAT or SDPT) for each year were estimated from the simulated 3-h series.

Two 75-year periods were defined, one in historical/current climate (1956–2030) (hereafter referred as historical climate or period) and one for the future period (2025–2099) with a 5-year overlapping period (2025–2030). Each grid point was analyzed by pooling the nine neighboring grid points in a configuration of 3 × 3 around the central analysis grid point. The spatial pooling was applied to reduce the uncertainties due to sampling when estimating the GEV parameters (Li, Zwiers, Zhang, & Li, 2019).

May to September 1, 6, 12, and 24 h annual maximum precipitation at each grid point were then extracted and normalized by the median value over each period. Normalized precipitation series were then fitted to a GEV distribution (see Section S2) using seasonal temperature anomalies as covariates for the GEV parameters. More specifically, grid-point May to September mean SAT or SDPT anomalies from each member over the two periods were considered as temperature covariates (T) for the local GEV location (μ) and log scale ($\log\sigma$) parameters. No dependence to covariate was assumed for the shape (ξ) parameter. Temperature covariate, either SAT or SDPT anomalies, is, therefore, local and more closely relates to the seasonal temperature anomalies driving local changes in extreme precipitation. This approach differs from Li, Zwiers, Zhang, and Li (2019), where the global annual mean temperature was used as temperature covariate.

Three models were considered relating GEV parameters to temperature: (a) M_0: stationary ($\mu(T) = \mu$; $\sigma(T) = \sigma$; $\xi(T) = \xi$); (b) M_1: location parameter linearly dependent on temperature covariate ($\mu(T) = \mu_0 + \mu_1 T$; $\sigma(T) = \sigma$; $\xi(T) = \xi$); and (c) M_2: location and log of the scale parameters linearly dependent on temperature covariate ($\mu(T) = \mu_0 + \mu_1 T$; $\log\sigma(T) = \sigma_0 + \sigma_1 T$; $\xi(T) = \xi$). The GEV parameters were estimated using Maximum Likelihood Estimation (MLE) and the likelihood ratio test was used (5% significance level) to compare the three models (Coles, 2001). The rate of change in return levels for different percentiles (e.g., 50th or 2-year event and 99th or 100-year event) was estimated for each member and each grid-point. The following expression which relates (in this case) changes in return levels from P_1 to P_2 to changes in temperature anomalies from T_1 to T_2 was used to estimate the scaling rate α (Hardwick Jones et al., 2010):

$$P_2 = P_1(1 + 0.01\alpha)^{(T_2 - T_1)} \quad (1)$$

Grid-point TPSR corresponds to the ensemble mean of the estimated α over the 50-member ensemble.

2.3. Temperature-Precipitation Scaling Rate Uncertainty

The robustness of TPSR estimates was assessed using the classification proposed by Li, Zwiers, Zhang, and Li (2019) based on the scaling rate per standard error ($SRSE$), which is estimated by dividing the TPSR by the standard deviation of α_i ($i = 1, ..., 50$) scaled by $1 / \sqrt{50}$. These authors classified the TPSR as *unconstrainable* when the $|SRSE| \leq 2$, *constrainable* when $2 < |SRSE| \leq 5$ and *robustly constrained* when $|SRSE| > 5$. *Robustly constrained* TPSR means that a significant response of extreme precipitation to temperature can be detected

through the scaling rate and that the corresponding TPSR can be tightly estimated. In contrast, an *unconstrainable* TPSR means that natural variability prevents the detection of any robust response of extreme precipitation to temperature changes. Various pooling strategies have been shown to improve the statistical significance of the TPSR estimates (Li, Zwiers, Zhang, & Li, 2019). Two pooling strategies were considered (3×3 and 5×5) but only results based on the 3×3 pooling strategy are presented in the following.

2.4. Projecting Future Extreme Precipitation Using Temperature-Precipitation Scaling Rate

To see if future extreme precipitation can be projected from TPSR estimated in historical period, TPSR values over historical and future periods were compared. Similar grid-point TPSR values over both periods were interpreted as indicative that projected extreme precipitation in future periods can be estimated from grid-point TPSR values in historical climate. Therefore, non-stationary models using dew-point temperature covariate can be used to assess projected changes in extreme precipitation. Mean grid-point TPSR values over each period were compared and the statistical significance (at a 95% confidence level) of these differences was assessed using the bootstrap approach (Efron & Tibshirani, 1993) (see Section S3).

3. Results and Discussion

3.1. Selected Non-Stationary GEV Distributions

The three GEV models were compared and the percentages of grid points where each model was selected were estimated for each simulation. The analysis was carried out for each duration (1, 6, 12, and 24 h), both periods and each temperature covariate (SAT or SDPT). Results show that non-stationary M_1 and M_2 models were selected at almost all grid points for both SAT and SDPT covariates, each period and all durations (see Figure S1). Stationary model M_0 was selected for less than 2% of the land grid-points. Since models M_0 and M_1 are particular cases of M_2, model M_2 was therefore considered in the following.

Temperature dependence (SAT or SDPT) on both GEV location and scaling parameters means that TPSR rates depend on precipitation percentiles as well as on temperature. This would not be the case if only the GEV location parameter was temperature dependant (e.g., Ali et al., 2018) where the TPSR would be the same for all extreme precipitation percentiles. However, as shown by Li, Zwiers, Zhang, and Li (2019), the sensitivity of TPSR to temperature is small when scale and/or shape parameters are temperature dependent.

3.2. Estimated Temperature-Precipitation Scaling Rates

Figure 2 displays the maps of the grid-point TPSR values for the 1 and 24 h 99th percentile precipitation over the domain for the historical period as well as the changes between the future and historical periods for SAT and SDPT covariates (Figure S2 presents the corresponding results for the 50th percentile precipitation). Strictly positive TPSR values are obtained for SDPT over the entire domain for both durations and periods. In contrast, lower TPSR values are observed for SAT and some regions even display negative values, especially in the southern part of the domain. These differences are even larger for the 50th percentile extreme precipitation (see Figure S2). Large increases in future TPSR values are observed for SAT, especially in the south-west part of the domain, while changes are smaller and randomly distributed for SDPT. The 24 h TPSR estimates using SAT are smaller than 1 h TPSR over the entire domain. Similar results were obtained for 6 and 12 h (see Figures S3 and S4 for 50th and 99th percentile precipitation, respectively).

Figure 3 presents the corresponding longitudinal distribution of 1 and 24 h TPSR for SAT and SDPT in historical and future periods for the 50th and 99th percentile precipitation. It clearly shows that the differences between TPSR using SAT or SDPT increase moving southward. Similar results can also be observed for the 24 h TPSR as well as for 6 and 12 h TPSR (see Figure S5). TPSR for 1 h precipitation using SDPT changes moving southward from values around the CC scaling to values above the CC scaling for both percentiles. A similar response is observed for 24 h precipitation with smaller TPSR values (below the CC scaling) in the northern and central parts of the domain. The estimated scaling rates using SAT are smaller than the

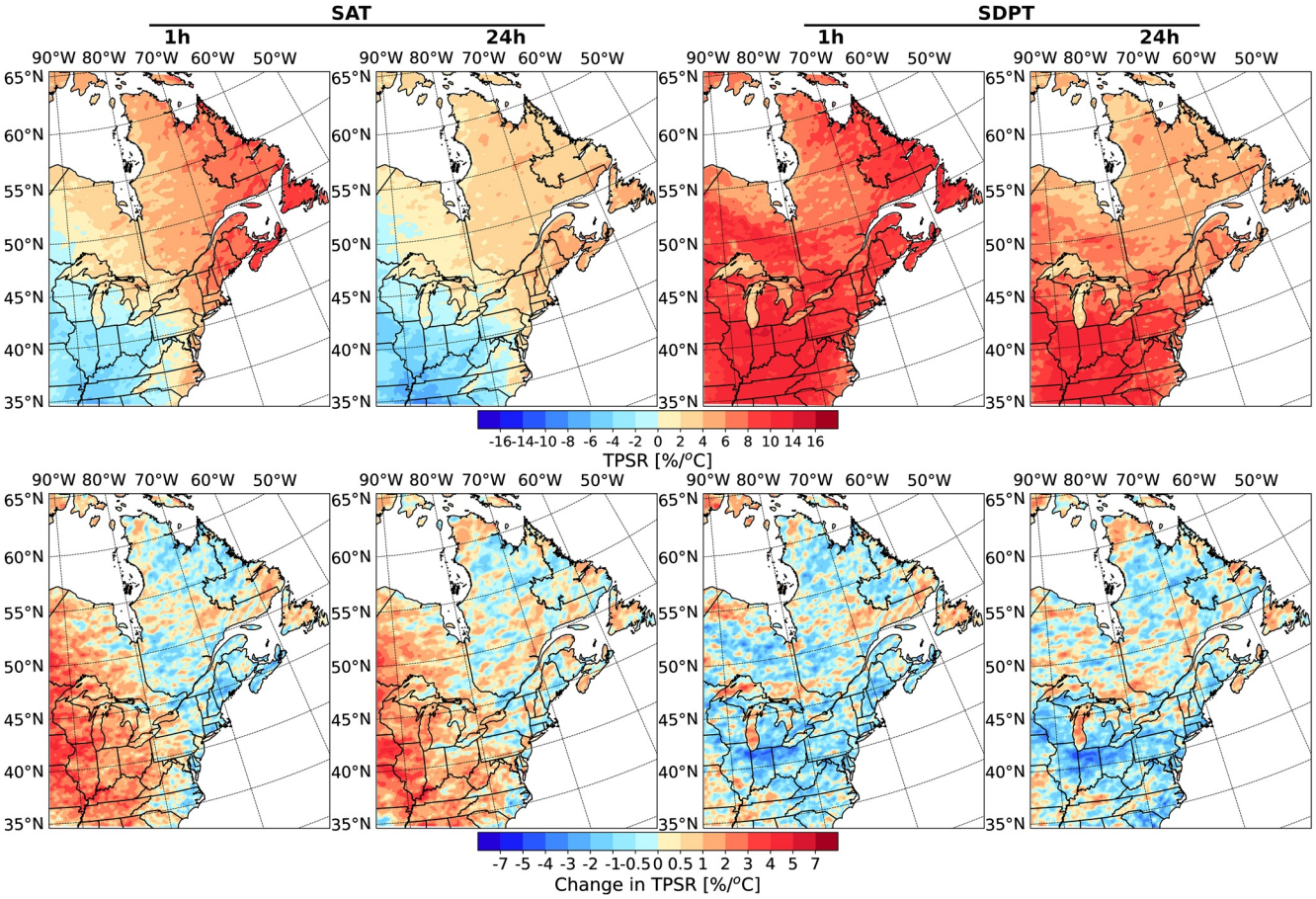

Figure 2. Temperature-precipitation scaling rate (TPSR) (%/°C) for the 99th percentile precipitation using surface air temperature (first two columns) and surface dew-point temperature (last two columns) as covariate over the period 1956–2030 (first row) and changes in TPSR (%/°C) between future (2025–2099) and historical period (1956–2030) (second row) for 1 h precipitation (first and third columns) and 24 h precipitation (second and fourth columns).

CC scaling over the vast majority of the domain and decrease as moving southward, even reaching negative TPSR for the southernmost part of the domain.

These differences in TPSR using SAT or SDPT clearly show that the available humidity is a limiting factor in the southern part of the domain and can even result in negative TPSR when SAT is considered. These results support the previously reported conclusion that SDPT is a better covariate to assess possible changes in daily and sub-daily extreme precipitation (e.g., Ali et al., 2018; Barbero et al., 2018; Wasko et al., 2018; W. Zhang et al., 2019). It also shows that negative scaling rates in the southern part of the domain are related to moisture availability and atmospheric circulation limiting the transport of moisture in these regions. Although negative scaling was not observed by Pall et al. (2007), these authors linked lower scaling rates in inland regions to the ability of the atmosphere to transport moisture to these regions. These results show that changes in relative humidity are an essential driver of TPSR (Barbero et al., 2018).

Smaller TPSR values for 24 h precipitation compared to 1 h precipitation in the northern part for both SAT and SDPT may also be due to changes in large-scale circulation (Magan et al., 2020) that might be responsible for moving the atmospheric moisture sources and changed the 24 h precipitation response in these regions. Further analysis would be needed to confirm this hypothesis. Super CC scaling is also observed for both 1 and 24 h extreme precipitation in the southern part of the domain for SDPT where it reaches values close to $12\%/°C$. In these regions, the extremes of precipitation may be less related to the increase in atmospheric moisture content (thermodynamic component) and more associated with changes in atmospheric motion and increases in vertical velocities (dynamic component). Therefore, super CC scaling may result from the dynamic nature of the temperature-moisture interaction related to feedback between precipitation

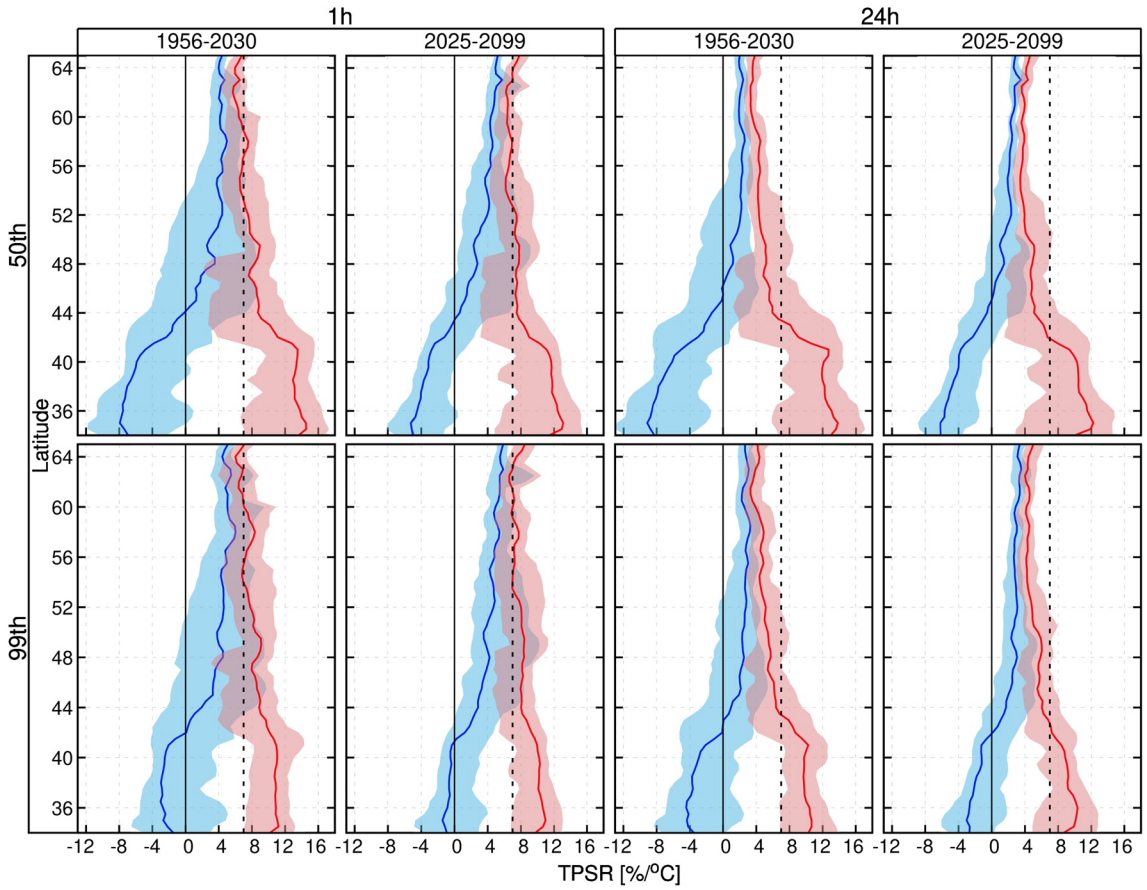

Figure 3. Longitudinal distribution of temperature-precipitation scaling rate values (%/°C) for the 50th percentile (first row) and the 99th percentile precipitation (second row) using surface air temperature (blue) or surface dew-point temperature (red) in historical (columns 1 and 3) and future periods (columns 2 and 4) for 1 h (columns 1 and 2) and 24 h (columns 3 and 4). Solid blue and red lines represent the median value, and the shaded regions represent the $5^{th}95^{th}$ percentile intervals. The vertical black line corresponds to 0, and the dashed vertical black line to the CC scaling (7%/°C). Latitude bins are 1° wide and are overlapping over 0.5°.

formation involving latent heat release and low-level moisture convergence (e.g., Trenberth et al., 2003; Westra et al., 2014). These results suggest that the response of extreme precipitation to changes in SDPT is dominantly thermodynamic over the central and northern regions of the domain and dominantly dynamic for the southern regions. Further studies are needed to assess the impact of dynamic circulation on extreme precipitation events and confirm this hypothesis.

3.3. Temperature-Precipitation Scaling Rate Dependence on Duration and Percentiles

The dependence of TPSR on precipitation duration and intensity was investigated. Figure 4 presents the distributions of TPSR values over the domain for the 99th percentile precipitation as a function of duration (similar results are obtained for the 50th percentile precipitation; see Figure S6). It demonstrates that temperature scaling is higher for shorter precipitation events with very similar distributions in future and historical periods. As previously mentioned, for SDPT, super CC scaling is observed over a majority of grid points for 1 h precipitation. It decreases as duration increase to a median TPSR value slightly below the CC scaling for 24 h precipitation. Therefore, shorter events will be more impacted by climate change, a result already reported in previous studies (e.g., Cannon & Innocenti, 2019; Innocenti, Mailhot, Leduc, et al., 2019; Li, Zwiers, Zhang, Chen, et al., 2019; Prein et al., 2017).

The dependence of TPSR on precipitation percentiles was analyzed by taking the difference between the TPSR values of various precipitation percentiles and the corresponding 50th percentile values at each grid

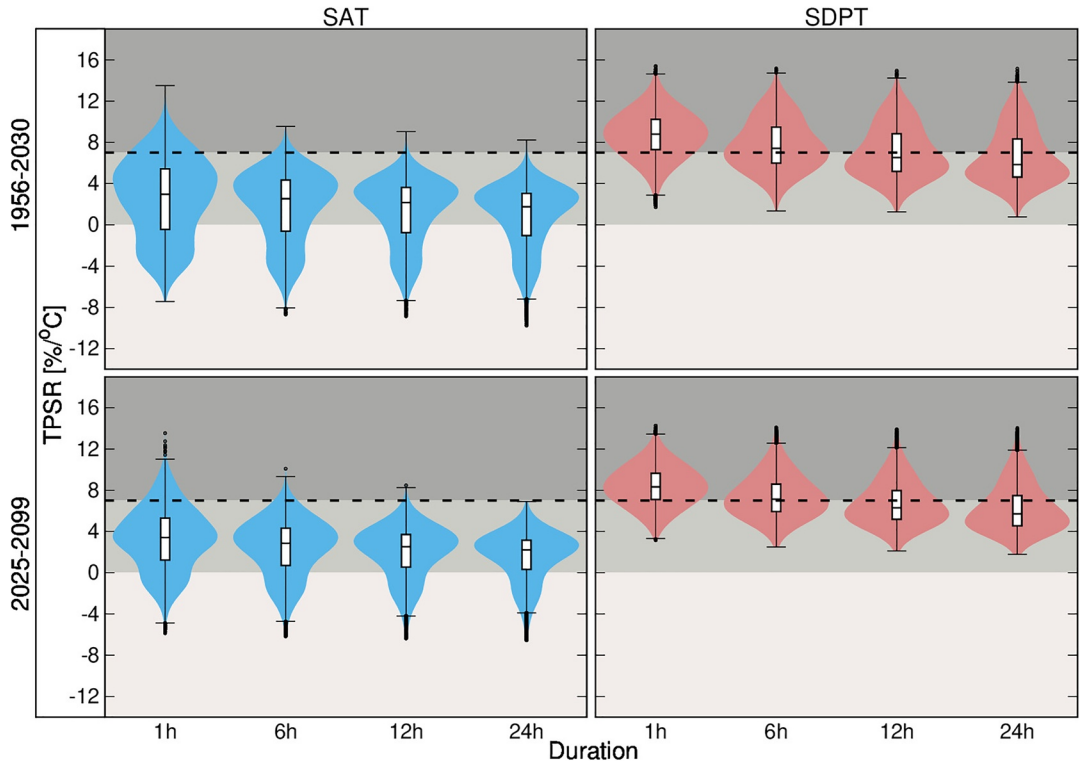

Figure 4. Distribution of temperature-precipitation scaling rate values (%/°C) for the 99th percentile precipitation using surface air temperature (blue) or surface dew-point temperature (red) in historical (top row) and future periods (bottom row) as a function of duration. The dashed horizontal line corresponds to the CC scaling (7%/°C).

point. The distributions of these differences are shown in Figure 5 for 1 h precipitation (Figure S7 shows corresponding figures for 24 h precipitation). Minimal increases in TPSR are observed for SDPT for more extreme precipitation over historical and future periods, while SAT increases are more pronounced. Corresponding maps displaying the grid point differences between 99th and 50th percentiles are showed in Figure 6. The SAT and SDPT display contrasting patterns in terms of expected TPSR changes across percentiles. For SAT, changes are positive on almost all the domain with higher values in the southern part. The patterns are very similar in historical and future periods and for both 1 and 24 h. The situation is radically different for SDPT, where the domain is divided in two, the northern part with positive changes and the southern part with negative changes. The coastal region in the southern part of the domain also displays positive changes between 99th and 50th percentiles, suggesting increasing scaling rates on coastal areas for more extreme precipitation.

How can these differences between SAT and SDPT be interpreted? Li, Zwiers, Zhang, Chen, et al. (2019), analyzing the relative contribution of dynamic and thermodynamic to the total scaling rate, using global surface temperature anomalies as covariate, concluded that the thermodynamic scaling rates remain almost unchanged with precipitation intensity and that circulation changes module the thermodynamic influence on extreme precipitation. Their results and those of Li, Zwiers, Zhang, and Li (2019) are similar to those obtained in this study and show increasing TPSR when SAT is considered, either at a local or global scale. The fact that more consistent results are obtained when using SDPT as covariate suggests that it partly captures the impacts of atmospheric circulation on moisture content and its effects on extreme precipitation events of different intensities (Barbero et al., 2018; Li, Zwiers, Zhang, & Li, 2019). Regions displaying positive changes in Figure 6, therefore, correspond to regions where moisture availability enables an increase in extreme precipitation events of different intensities while negative changes correspond to regions where atmospheric circulation weakens the thermodynamic response.

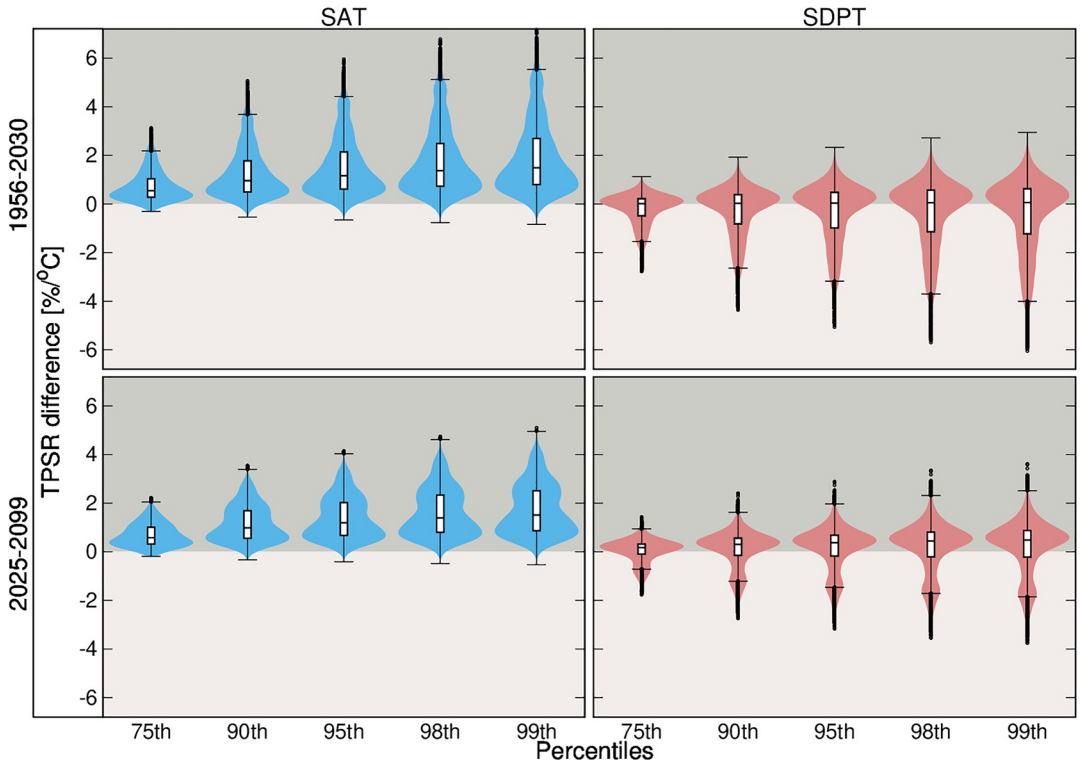

Figure 5. Distribution of the grid point difference between the temperature-precipitation scaling rate values for various precipitation percentiles and the 50th percentile values ([Xth percentile–50th percentile] in %/°C) for the 1 h precipitation using surface air temperature (blue) or surface dew-point temperature (red) in historical (top row) and future periods (bottom row) as a function of percentiles.

3.4. Robustness of Estimated Temperature-Precipitation Scaling Rates

Figure 7 shows the percentages of robustly constrained ($|SRSE| > 5$) grid points for each covariate, period, and duration for 50th and 99th percentiles. The fraction of robustly constrained TPSR is close to 100% for SDPT but much smaller for SAT and decreases in both cases as duration increases. It is also larger for the future period. These results indicate that the link between extreme precipitation and temperature changes is stronger for short-duration precipitation events and for the future period where the signal-to-noise ratio is larger. This link is also much stronger when SDPT is used as a covariate. It is interesting to note that this result is obtained using a local temperature covariate. It is also interesting to mention that dominantly robustly constrained TPSR are also obtained when using an at-site analysis (not shown here) instead of a 3 × 3 regional pooling.

3.5. Comparison of Temperature-Precipitation Scaling Rates in Future and Historical Periods

Figure 8 shows maps of land grid-points with significant and non-significant changes (95% confidence level) of the 1 h TPSR values between future and historical periods for 50th and 99th percentile precipitation for SAT and SDPT (Figure S8 presents the corresponding maps for 24 h extreme precipitation). It shows that TPSR values are similar in future and historical periods for nearly 87% of the grid points for the 99th percentile precipitation when using SDPT as covariate (these percentages remain almost unchanged across durations for a given precipitation percentile; see Figure S9). Smaller percentages (around 63%) are obtained for the 2-year event. Again, corresponding values for SAT are much smaller, suggesting that the scaling is more consistent and relevant when an estimate of humidity, as in SDPT, is introduced into the covariate (Barbero et al., 2018; Roderick et al., 2020; Wasko et al., 2018). Although TPSR is different from the CC scaling, results show consistent TPSR based on local seasonal SDPT anomalies between the historical and future period

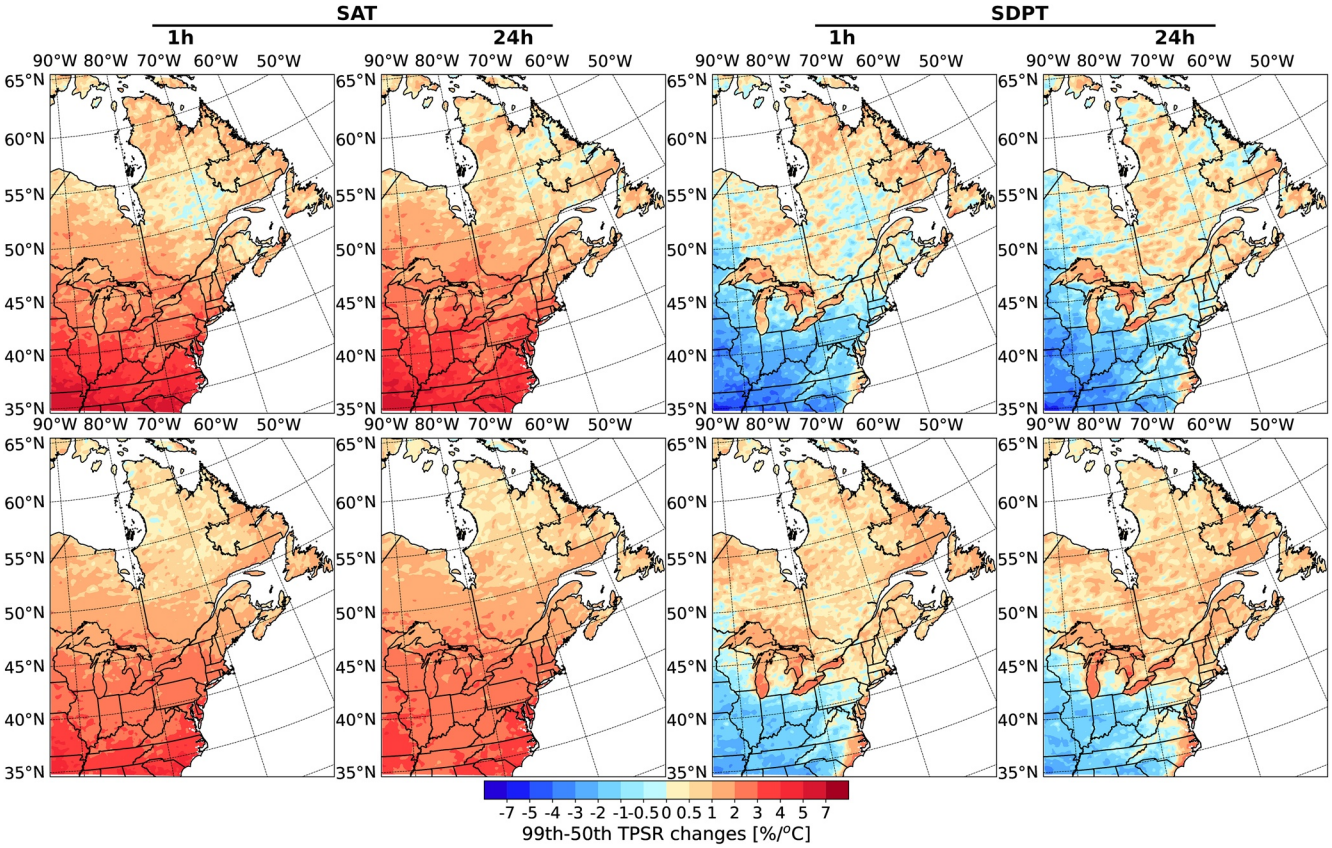

Figure 6. Maps of the differences between the 99th and 50th precipitation percentiles temperature-precipitation scaling rate values in %/°C using surface air temperature (first two columns) and surface dew-point temperature (last two columns) as covariate over the period 1956–2030 (first row) and 2025–2099 (second row) for 1 h precipitation (first and third columns) and 24 h precipitation (second and fourth columns).

over a large part of the domain. Therefore, historical TPSR for a specific duration and percentiles can be used to assess projected changes of corresponding extreme precipitation.

Results are not very sensitive to the duration for a given precipitation intensity (see Figure S9). However, large increases in percentages of land grid points with non-significant TPSR changes between future and historical periods are observed as more extreme precipitation is considered (see Figure S9). Again, they reflect the dominant role of temperature and moisture availability, embedded in SDPT, as explanatory variables of the projected changes for the most extreme precipitation.

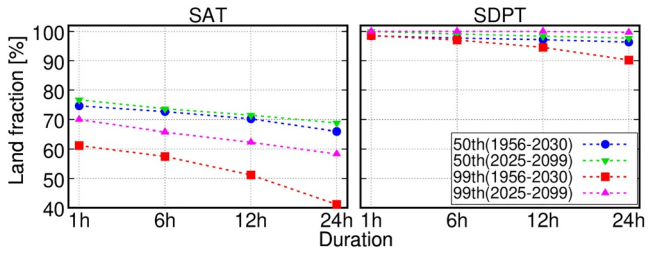

Figure 7. Percentages of land grid points with robustly constrained ($|SRSE| > 5$) temperature-precipitation scaling rate as a function of durations for both periods, 50th and 99th percentile precipitation, surface air temperature (left panel), and surface dew-point temperature (right panel).

4. Conclusions

Extreme precipitation response to changes in SAT and SDPT over the Northeastern North America region has been investigated using the 50-member ensemble from the fifth version of the CRCM5-LE based on RCP8.5. The simulated 1, 6, 12, and 24 h May–September maximum precipitation were used in combination with the May–September local mean temperature (SAT and SDPT) anomalies for each year of the 1956–2030 and 2025–2099 periods to estimate the TPSRs. A non-stationary GEV model with a linear dependence to covariate (SAT and SDPT) for both location and the log of the scale parameters was considered. Grid-point TPSRs were estimated for each CRCM5 simulation and averaged over the 50 members. A 3×3 pooling strategy was used to improve the sampling.

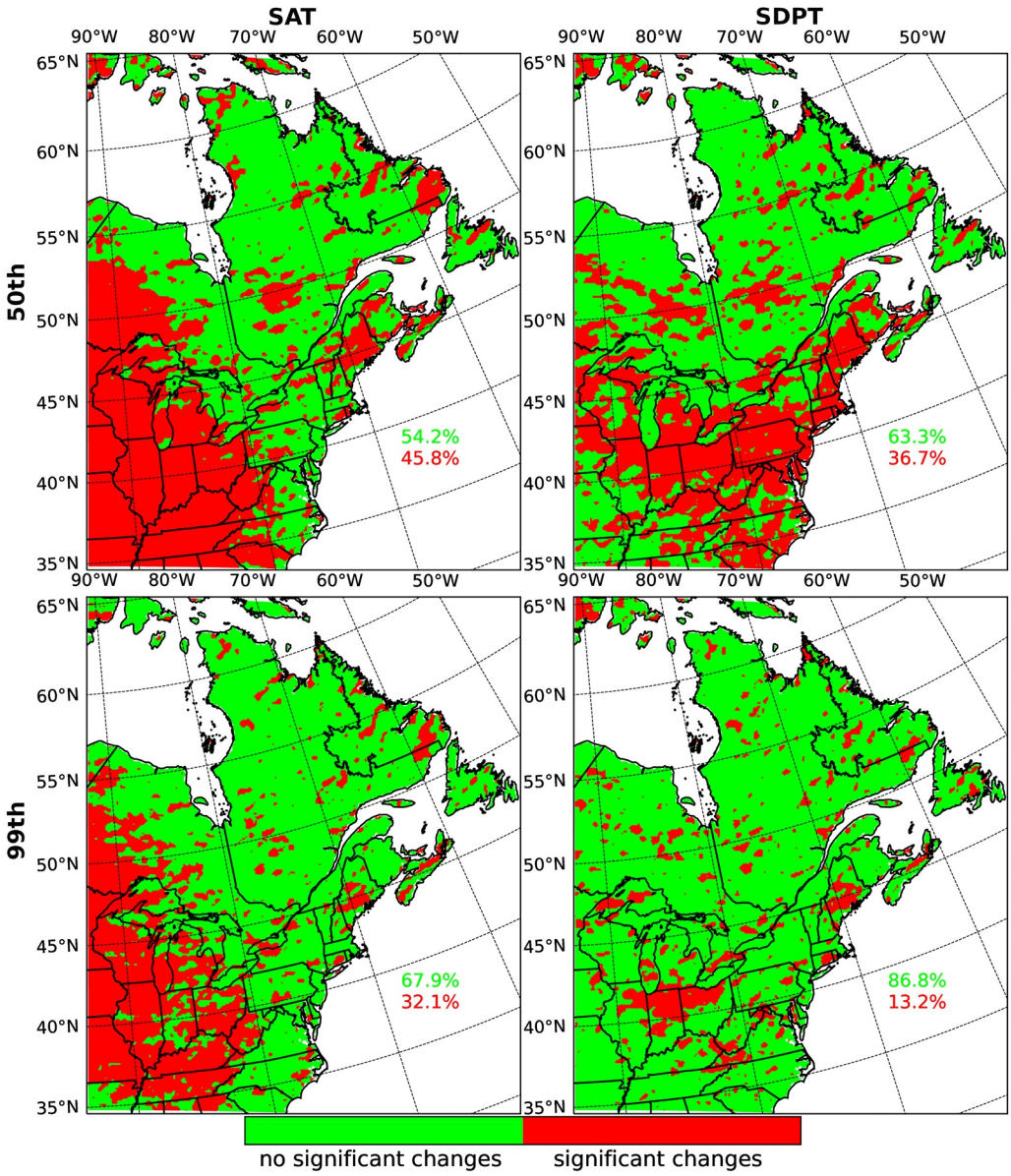

Figure 8. Land grid points with significant and non significant changes in 1 h temperature-precipitation scaling rate between future and historical periods for the 50th (top row) and 99th percentile (bottom row) precipitation using surface air temperature (left column) and surface dew-point temperature (right column). The numbers in the map correspond to the percentage of land grid points of each category.

Very different results were obtained for TPSR based on SAT or SDPT. If TPSR is close or slightly smaller than CC scaling in the northern part of the domain, contrasting responses for SAT and SDPT are observed moving southward for all durations and precipitation intensities. Thus, if TPSR based on SDPT progressively increases to reach super CC scaling in the southernmost part of the domain, TPSR based on SAT decrease and display negative values over the southern regions. Available humidity is clearly a limiting factor in these regions as atmospheric circulation limits moisture transport, explaining these contrasting responses between SAT and SDPT scaling rates.

Scaling rates are also generally lower for longer durations compared to 1 h precipitation, especially in the northern part of the domain, and may be related to the plausibly more dominant role of atmospheric circulation for longer duration extreme precipitation. Shorter extreme precipitation is, therefore, more impacted by climate change. Super CC scaling observed in the southern part of the domain for SDPT may be related

to the dynamic of convective events over these regions (latent heat release intensifying the updrafts on convective clouds) (Lenderink & Meijgaard, 2009, 2010; Trenberth et al., 2003).

Changes in TPSR with precipitation intensities were also investigated and reveals the regional differences in moisture availability and its role in the T-P relationship for more extreme precipitation. It suggests that the TPSR estimated with SDPT somewhat captures, even partly, the influence of atmospheric circulation on humidity and its impact on precipitation events at different intensities over the durations considered.

The robustness of the TPSR estimates was evaluated over the entire domain. The TPSR estimated using SDPT was more robustly constrained (above 90% of grid points for all the cases) regardless of the percentile, duration, or study period compared to TPSR based on SAT. Thus, the link between extreme precipitation and SDPT changes is stronger and less affected by internal variability for short-duration precipitation events and for the future period where the signal-to-noise ratio is highest.

Comparison of TPSR in historical and future periods shows that the TPSR remains unchanged (at the 95% confidence level) in future climate for more extreme precipitation over large parts of the domain. It is especially for SDPT, where around 87% of TPSR land grid point values remain unchanged for the 100-year 1 h extreme precipitation. The percentages of unchanged values increase for more extreme precipitation but remain almost similar over durations.

These results confirm the importance of using the SDPT over the SAT in TPSR estimation. Estimated scaling rates based on SDPT take into consideration dynamical effects related to moisture availability. It results in more robustly constrained TPSR values, scaling rates closer to the CC scaling, and more consistent values in historical and future climate over a larger part of the simulation domain. Therefore, historical TPSR based on SDPT can assess the projected changes in extreme precipitation more robustly. These results are important as they can help provide guidelines to the engineering community to project future design values related to extreme precipitation more reliably. Future work intends to further investigate how the scaling changes when only the convective precipitation component is considered.

Acknowledgments
The authors would like to thank the anonymous reviewers who, thanks to their comments, helped to improve the quality of the manuscript. A. Mailhot thanks to the Discovery Grants Program from the Natural Science and Engineering Research Council of Canada (NSERC) for providing financial support for this project. The authors thank the consortium Ouranos who gave access to the CRCM5-LE. The production of ClimEx was funded within the ClimEx project by the Bavarian State Ministry for the Environment and Consumer Protection. The CRCM5 was developed by the ESCER Center of Université du Québec à Montréal (UQAM) in collaboration with Environment and Climate Change Canada. The authors acknowledge Environment and Climate Change Canada's Canadian Center for Climate Modeling and Analysis for executing and making available the CanESM2 Large Ensemble simulations for the ClimEx project, and the Canadian Sea Ice and Snow Evolution Network for proposing the simulations. Computations with the CRCM5 for the ClimEx project were made on the SuperMUC supercomputer at Leibniz Supercomputing Center (LRZ) of the Bavarian Academy of Sciences and Humanities. The operation of this supercomputer is funded via the Gauss Center for Supercomputing (GCS) by the German Federal Ministry of Education and Research and the Bavarian State Ministry of Education, Science and the Arts.

Data Availability Statement

The CRCM5-LE data set can be obtained online (https://www.climex-project.org/en/data-access).

References

Alduchov, O. A., & Eskridge, R. E. (1996). Improved Magnus form approximation of saturation vapor pressure. *Journal of Applied Meteorology*, *35*(4), 601–609. https://doi.org/10.1175/1520-0450(1996)035<0601:imfaos>2.0.co;2

Alexander, L. V., Zhang, X., Peterson, T. C., Caesar, J., Gleason, B., Klein Tank, A. M. G., et al. (2006). Global observed changes in daily climate extremes of temperature and precipitation. *Journal of Geophysical Research*, *111*, D05109. https://doi.org/10.1029/2005JD006290

Ali, H., Fowler, H. J., & Mishra, V. (2018). Global observational evidence of strong linkage between dew point temperature and precipitation extremes. *Geophysical Research Letters*, *45*(22), 12320–12330. https://doi.org/10.1029/2018GL080557

Arora, V. K., Scinocca, J. F., Boer, G. J., Christian, J. R., Denman, K. L., Flato, G. M., et al. (2011). Carbon emission limits required to satisfy future representative concentration pathways of greenhouse gases. *Geophysical Research Letters*, *38*(5), L05805. https://doi.org/10.1029/2010GL046270

Bao, J., Sherwood, S. C., Alexander, L. V., & Evans, J. P. (2017). Future increases in extreme precipitation exceed observed scaling rates. *Nature Climate Change*, *7*(2), 128–132. https://doi.org/10.1038/nclimate3201

Barbero, R., Westra, S., Lenderink, G., & Fowler, H. J. (2018). Temperature-extreme precipitation scaling: A two-way causality? *International Journal of Climatology*, *38*, e1274–e1279. https://doi.org/10.1002/joc.5370

Berg, P., Haerter, J. O., Thejll, P., Piani, C., Hagemann, S., & Christensen, J. H. (2009). Seasonal characteristics of the relationship between daily precipitation intensity and surface temperature. *Journal of Geophysical Research*, *114*, D18102. https://doi.org/10.1029/2009JD012008

Cannon, A. J., & Innocenti, S. (2019). Projected intensification of sub-daily and daily rainfall extremes in convection-permitting climate model simulations over North America: Implications for future intensity-duration-frequency curves. *Natural Hazards and Earth System Sciences*, *19*(2), 421–440. https://doi.org/10.5194/nhess-19-421-2019

Coles, S. (2001). *An introduction to statistical modeling of extreme values*. Springer-Verlag. https://doi.org/10.1007/978-1-4471-3675-0

Donat, M. G., Alexander, L. V., Yang, H., Durre, I., Vose, R., Dunn, R. J. H., et al. (2013). Updated analyses of temperature and precipitation extreme indices since the beginning of the twentieth century: The HadEX2 dataset. *Journal of Geophysical Research: Atmospheres*, *118*(5), 2098–2118. https://doi.org/10.1002/jgrd.50150

Efron, B., & Tibshirani, R. J. (1993). *An introduction to the bootstrap (No. 57)*. Chapman & Hall/CRC.

Emori, S., & Brown, S. J. (2005). Dynamic and thermodynamic changes in mean and extreme precipitation under changed climate. *Geophysical Research Letters*, *32*, L17706. https://doi.org/10.1029/2005GL023272

Fischer, E. M., & Knutti, R. (2016). Observed heavy precipitation increase confirms theory and early models. *Nature Climate Change*, *6*(11), 986–991. https://doi.org/10.1038/nclimate3110

Frich, P., Alexander, L. V., DellaMarta, P., Gleason, B., Haylock, M., Tank, A. M. G. K., & Peterson, T. (2002). Observed coherent changes in climatic extremes during the second half of the twentieth century. *Climate Research*, *19*(3), 193–212. https://doi.org/10.3354/cr019193

Fyfe, J. C., Derksen, C., Mudryk, L., Flato, G. M., Santer, B. D., Swart, N. C., et al. (2017). Large near-term projected snowpack loss over the western United States. *Nature Communications*, *8*, 14996. https://doi.org/10.1038/ncomms14996

Gutowski, W. J., Takle, E. S., Kozak, K. A., Patton, J. C., Arritt, R. W., & Christensen, J. H. (2007). A possible constraint on regional precipitation intensity changes under global warming. *Journal of Hydrometeorology*, *8*(6), 1382–1396. https://doi.org/10.1175/2007JHM817.1

Hardwick Jones, R., Westra, S., & Sharma, A. (2010). Observed relationships between extreme sub-daily precipitation, surface temperature, and relative humidity. *Geophysical Research Letters*, *37*(22), L22805. https://doi.org/10.1029/2010GL045081

Innocenti, S., Mailhot, A., Frigon, A., Cannon, A. J., & Leduc, M. (2019). Observed and simulated precipitation over northeastern North America: How do daily and subdaily extremes scale in space and time? *Journal of Climate*, *32*(24), 8563–8582. https://doi.org/10.1175/JCLI-D-19-0021.1

Innocenti, S., Mailhot, A., Leduc, M., Cannon, A. J., & Frigon, A. (2019). Projected changes in the probability distributions, seasonality, and spatiotemporal scaling of daily and subdaily extreme precipitation simulated by a 50-member ensemble over northeastern North America. *Journal of Geophysical Research: Atmospheres*, *124*(19), 10427–10449. https://doi.org/10.1029/2019JD031210

IPCC. (2014). Climate change 2014: Synthesis report. In R. K. Pachauri, L. A. Meyer (Eds.), & Core Writing Team. (Eds.), *Contribution of working groups I, II and III to the fifth assessment report of the intergovernmental panel on climate change* (p. 151). IPCC.

Kharin, V. V., Zwiers, F. W., Zhang, X., & Wehner, M. (2013). Changes in temperature and precipitation extremes in the CMIP5 ensemble. *Climatic Change*, *119*(2), 345–357. https://doi.org/10.1007/s10584-013-0705-8

Lawrence, M. G. (2005). The relationship between relative humidity and the dewpoint temperature in moist air: A simple conversion and applications. *Bulletin of the American Meteorological Society*, *86*(2), 225–234. https://doi.org/10.1175/BAMS-86-2-225

Leduc, M., Mailhot, A., Frigon, A., Martel, J.-L., Ludwig, R., Brietzke, G. B., et al. (2019). The ClimEx project: A 50-member ensemble of climate change projections at 12-km resolution over Europe and northeastern North America with the Canadian regional climate model (CRCM5). *Journal of Applied Meteorology and Climatology*, *58*(4), 663–693. https://doi.org/10.1175/JAMC-D-18-0021.1

Lenderink, G., & Attema, J. (2015). A simple scaling approach to produce climate scenarios of local precipitation extremes for the Netherlands. *Environmental Research Letters*, *10*(8), 085001. https://doi.org/10.1088/1748-9326/10/8/085001

Lenderink, G., Barbero, R., Loriaux, J. M., & Fowler, H. J. (2017). Super-Clausius-Clapeyron scaling of extreme hourly convective precipitation and its relation to large-scale atmospheric conditions. *Journal of Climate*, *30*(15), 6037–6052. https://doi.org/10.1175/JCLI-D-16-0808.1

Lenderink, G., de Vries, H., Fowler, H. J., Barbero, R., van Ulft, B., & van Meijgaard, E. (2021). Scaling and responses of extreme hourly precipitation in three climate experiments with a convection-permitting model. *Philosophical Transactions of the Royal Society A: Mathematical, Physical & Engineering Sciences*, *379*(2195), 20190544. https://doi.org/10.1098/rsta.2019.0544

Lenderink, G., & Meijgaard, E. (2008). Increase in hourly precipitation extremes beyond expectations from temperature changes. *Nature Geoscience*, *1*(8), 511–514. https://doi.org/10.1038/ngeo262

Lenderink, G., & Meijgaard, E. V. (2009). Unexpected rise in extreme precipitation caused by a shift in rain type? *Nature Geoscience*, *2*(6), 373. https://doi.org/10.1038/ngeo524

Lenderink, G., & Meijgaard, E. V. (2010). Linking increases in hourly precipitation extremes to atmospheric temperature and moisture changes. *Environmental Research Letters*, *5*(2), 025208. https://doi.org/10.1088/1748-9326/5/2/025208

Lenderink, G., Mok, H. Y., Lee, T. C., & Oldenborgh, G. J. V. (2011). Scaling and trends of hourly precipitation extremes in two different climate zones—Hong Kong and the Netherlands. *Hydrology and Earth System Sciences*, *15*(9), 3033–3041. https://doi.org/10.5194/hess-15-3033-2011

Li, C., Zwiers, F., Zhang, X., Chen, G., Lu, J., Li, G., et al. (2019). Larger increases in more extreme local precipitation events as climate warms. *Geophysical Research Letters*, *46*, 6885–6891. https://doi.org/10.1029/2019GL082908

Li, C., Zwiers, F., Zhang, X., & Li, G. (2019). How much information is required to well constrain local estimates of future precipitation extremes? *Earth's Future*, *7*(1), 11–24. https://doi.org/10.1029/2018EF001001

Li, C., Zwiers, F., Zhang, X., Li, G., Sun, Y., & Wehner, M. (2021). Changes in annual extremes of daily temperature and precipitation in CMIP6 models. *Journal of Climate*, *34*(9), 3441–3460. https://doi.org/10.1175/JCLI-D-19-1013.1

Magan, B., Kim, S., Wasko, C., Barbero, R., Moron, V., Nathan, R., & Sharma, A. (2020). Impact of atmospheric circulation on the rainfall-temperature relationship in Australia. *Environmental Research Letters*, *15*(9), 094098. https://doi.org/10.1088/1748-9326/abab35

Mailhot, A., Beauregard, I., Talbot, G., Caya, D., & Biner, S. (2011). Future changes in intense precipitation over Canada assessed from multi-model NARCCAP ensemble simulations. *International Journal of Climatology*, *32*(8), 1151–1163. https://doi.org/10.1002/joc.2343

Martel, J.-L., Mailhot, A., & Brissette, F. (2020). Global and regional projected changes in 100-yr subdaily, daily, and multiday precipitation extremes estimated from three large ensembles of climate simulations. *Journal of Climate*, *33*(3), 1089–1103. https://doi.org/10.1175/JCLI-D-18-0764.1

Martinkova, M., & Kysely, J. (2020). Overview of observed Clausius-Clapeyron scaling of extreme precipitation in midlatitudes. *Atmosphere*, *11*(6), 786. https://doi.org/10.3390/atmos11080786

Martynov, A., Laprise, R., Sushama, L., Winger, K., Šeparović, L., & Dugas, B. (2013). Reanalysis-driven climate simulation over CORDEX North America domain using the Canadian regional climate model, version 5: Model performance evaluation. *Climate Dynamics*, *41*(11), 2973–3005. https://doi.org/10.1007/s00382-013-1778-9

Min, S.-K., Zhang, X., Zwiers, F. W., & Hegerl, G. C. (2011). Human contribution to more-intense precipitation extremes. *Nature*, *470*(7334), 378–381. https://doi.org/10.1038/nature09763

Molnar, P., Fatichi, S., Gaál, L., Szolgay, J., & Burlando, P. (2015). Storm type effects on Super Clausius-Clapeyron scaling of intense rainstorm properties with air temperature. *Hydrology and Earth System Sciences*, *19*(4), 1753–1766. https://doi.org/10.5194/hess-19-1753-2015

Norris, J., Chen, G., & Neelin, J. D. (2019). Thermodynamic versus dynamic controls on extreme precipitation in a warming climate from the community Earth system model large ensemble. *Journal of Climate*, *32*(4), 1025–1045. https://doi.org/10.1175/JCLI-D-18-0302.1

O'Gorman, P. A. (2012). Sensitivity of tropical precipitation extremes to climate change. *Nature Geoscience*, *5*(10), 697–700. https://doi.org/10.1038/ngeo1568

O'Gorman, P. A., & Schneider, T. (2009). The physical basis for increases in precipitation extremes in simulations of 21st-century climate change. *Proceedings of the National Academy of Sciences of the United States of America*, *106*(35), 14773–14777. https://doi.org/10.1073/pnas.0907610106

Pall, P., Allen, M., & Stone, D. (2007). Testing the Clausius-Clapeyron constraint on changes in extreme precipitation under CO_2 warming. *Climate Dynamics*, *28*(4), 351–363. https://doi.org/10.1007/s00382-006-0180-2

Panthou, G., Mailhot, A., Laurence, E., & Talbot, G. (2014). Relationship between surface temperature and extreme rainfalls: A multi-time-scale and event-based analysis. *Journal of Hydrometeorology*, *15*(5), 1999–2011. https://doi.org/10.1175/JHM-D-14-0020.1

Park, I.-H., & Min, S.-K. (2017). Role of convective precipitation in the relationship between subdaily extreme precipitation and temperature. *Journal of Climate*, *30*(23), 9527–9537. https://doi.org/10.1175/JCLI-D-17-0075.1

Peleg, N., Marra, F., Fatichi, S., Molnar, P., Morin, E., Sharma, A., & Burlando, P. (2018). Intensification of convective rain cells at warmer temperatures observed from high-resolution weather radar data. *Journal of Hydrometeorology*, *19*(4), 715–726. https://doi.org/10.1175/JHM-D-17-0158.1

Pfahl, S., O'Gorman, P. A., & Fischer, E. M. (2017). Understanding the regional pattern of projected future changes in extreme precipitation. *Nature Climate Change*, *7*(6), 423–427. https://doi.org/10.1038/nclimate3287

Prein, A. F., Rasmussen, R. M., Ikeda, K., Liu, C. H., Clark, M. P., & Holland, G. J. (2017). The future intensification of hourly precipitation extremes. *Nature Climate Change*, *7*(1), 48–52. https://doi.org/10.1038/nclimate3168

Räisänen, J. (2007). How reliable are climate models? *Tellus*, *59*(1), 2–29. https://doi.org/10.1111/j.1600-0870.2006.00211.x

Roderick, T. P., Wasko, C., & Sharma, A. (2020). An improved covariate for projecting future rainfall extremes? *Water Resources Research*, *56*(8), e2019WR026924. https://doi.org/10.1029/2019WR026924

Separović, L., Alexandru, A., Laprise, R., Martynov, A., Sushama, L., Winger, K., et al. (2013). Present climate and climate change over North America as simulated by the fifth-generation Canadian regional climate model. *Climate Dynamics*, *41*(11), 3167–3201. https://doi.org/10.1007/s00382-013-1737-5

Sun, Q., Zhang, X., Zwiers, F., Westra, S., & Alexander, L. V. (2021). A global, continental, and regional analysis of changes in extreme precipitation. *Journal of Climate*, *34*(1), 243–258. https://doi.org/10.1175/JCLI-D-19-0892.1

Sun, Q., Zwiers, F., Zhang, X., & Li, G. (2020). A comparison of intra-annual and long-term trend scaling of extreme precipitation with temperature in a large-ensemble regional climate simulation. *Journal of Climate*, *33*(21), 9233–9245. https://doi.org/10.1175/JCLI-D-19-0920.1

Trenberth, K. E., Dai, A., Rasmussen, R. M., & Parsons, D. B. (2003). The changing character of precipitation. *Bulletin of the American Meteorological Society*, *84*(9), 1205–1218. https://doi.org/10.1175/BAMS-84-9-1205

Utsumi, N., Seto, S., Kanae, S., Maeda, E. E., & Oki, T. (2011). Does higher surface temperature intensify extreme precipitation? *Geophysical Research Letters*, *38*(16), L16708. https://doi.org/10.1029/2011GL048426

Visser, J. B., Wasko, C., Sharma, A., & Nathan, R. (2020). Resolving inconsistencies in extreme precipitation-temperature sensitivities. *Geophysical Research Letters*, *47*(18), e2020GL089723. https://doi.org/10.1029/2020GL089723

Wasko, C., Lu, W. T., & Mehrotra, R. (2018). Relationship of extreme precipitation, dry-bulb temperature, and dew point temperature across Australia. *Environmental Research Letters*, *13*(7), 074031. https://doi.org/10.1088/1748-9326/aad135

Wasko, C., & Sharma, A. (2014). Quantile regression for investigating scaling of extreme precipitation with temperature. *Water Resources Research*, *50*(4), 3608–3614. https://doi.org/10.1002/2013WR015194

Westra, S., Fowler, H. J., Evans, J. P., Alexander, L. V., Berg, P., Johnson, F., et al. (2014). Future changes to the intensity and frequency of short-duration extreme rainfall. *Reviews of Geophysics*, *52*(3), 522–555. https://doi.org/10.1002/2014RG000464

Zhang, W., Villarini, G., & Wehner, M. (2019). Contrasting the responses of extreme precipitation to changes in surface air and dew point temperatures. *Climatic Change*, *154*(1–2), 257–271. https://doi.org/10.1007/s10584-019-02415-8

Zhang, X., Zwiers, F. W., Li, G., Wan, H., & Cannon, A. J. (2017). Complexity in estimating past and future extreme short-duration rainfall. *Nature Geoscience*, *10*(4), 255–259. https://doi.org/10.1038/ngeo2911